In-gas-cell laser spectroscopy of the magnetic dipole moment of the N 126 isotope Pt199

doi: 10.1103/PhysRevC.96.014307

In-gas-cell laser spectroscopy of the magnetic dipole moment of the $N \approx 126$ isotope ^{199}Pt

Y. Hirayama,[1,*] M. Mukai,[1,2,3] Y. X. Watanabe,[1] M. Ahmed,[1,2] S. C. Jeong,[1,4] H. S. Jung,[1] Y. Kakiguchi,[1] S. Kanaya,[3,5] S. Kimura,[1,2,3] J. Y. Moon,[4] T. Nakatsukasa,[2] M. Oyaizu,[1] J. H. Park,[4] P. Schury,[1] A. Taniguchi,[6] M. Wada,[1,3] K. Washiyama,[2] H. Watanabe,[3,7] and H. Miyatake[1]

[1]*Wako Nuclear Science Center (WNSC), Institute of Particle and Nuclear Studies (IPNS), High Energy Accelerator Research Organization (KEK), Wako, Saitama 351-0198, Japan*

[2]*Graduate School of Pure and Applied Sciences, University of Tsukuba, Tsukuba, Ibaraki 305-0006, Japan*

[3]*Nishina Center for Accelerator-Based Science, RIKEN, Wako, Saitama 351-0198, Japan*

[4]*Rare Isotope Science Project, Institute for Basic Science (IBS), Daejeon 305-811, Republic of Korea*

[5]*Department of Physics, Osaka University, Toyonaka, Osaka 563-0043, Japan*

[6]*Research Reactor Institute, Kyoto University, Kumatori, Osaka, 590-0494, Japan*

[7]*IRCNPC, School of Physics and Nuclear Energy Engineering, Beihang University, Beijing 100191, China*

(Received 21 July 2016; revised manuscript received 28 May 2017; published 11 July 2017)

The magnetic dipole moment and mean-square charge radius of ^{199g}Pt ($I^\pi = 5/2^-$, $t_{1/2} = 30.8$ min) ground state and ^{199m}Pt ($E_{ex} = 424$ keV, $I^\pi = (13/2)^+$, $t_{1/2} = 13.6$ s) isomeric state are evaluated for the first time from investigations of the hyperfine splitting of the $\lambda_1 = 248.792$ nm transition by in-gas-cell laser ionization spectroscopy. Ground and isomeric states of neutron-rich ^{199}Pt nucleus were produced by a multinucleon transfer reaction at the KEK Isotope Separation System (KISS), designed for the study of nuclear spectroscopy in the vicinity of $N = 126$. The measured magnetic dipole moments $+0.75(8)\mu_N$ and $-0.57(5)\mu_N$ are consistent with the systematics of those of nuclei with $I^\pi = 5/2^-$ and $I^\pi = 13/2^+$, respectively.

DOI: 10.1103/PhysRevC.96.014307

I. INTRODUCTION

The allowed Gamow-Teller (GT) and first-forbidden (FF) β-decay transitions compete in nuclei around $N = 126$. The proton orbit of neutron-rich nuclei around $N = 126$ is $\pi(0h_{11/2})$ and hence the GT transition from $\nu(0h_{9/2})$ to $\pi(0h_{11/2})$ and the FF transition from $\nu(0i_{13/2})$ to $\pi(0h_{11/2})$ compete. This makes it difficult to predict nuclear properties such as half-lives and nuclear masses in neutron-rich nuclei around $N = 126$ using theoretical nuclear models [1–3]. For example, estimated half-lives of these nuclei typically differ by an order of magnitude [4–8]. The half-life is an important factor in investigations into astrophysical environments and nuclear structure. For example, the formation of the third peak in observed solar r-process abundance patterns is dependent on the half-life [9,10]. Also, the abundance peak height around $A = 195$ is proportional to the half-life, and the peak position and its width drastically change according to the half-life. Experimental nuclear spectroscopy can be used to eliminate uncertainty and improve predictions of nuclear properties by ensuring the FF transition is correctly accounted for.

The nuclear structure toward $N = 126$ can be revealed through electromagnetic moments [11] and has been intensively studied using various techniques. The nuclear wave function and shape can be evaluated from the magnetic dipole moment (μ) and electric quadrupole moment (Q), respectively. In particular, understanding the wave function in the ground state in this region is essential for accurate predictions of the GT and FF transition strengths and the β-decay half-life. However, the difficulty of obtaining nuclei in the vicinity of $N = 126$ has made it problematic to measure electromagnetic moments. To address this, we initiated the KEK Isotope Separation System (KISS) project [12] for selecting nuclei around $N = 126$ by an argon-gas-cell-based laser ion source combined with an online isotope separator [13,14]. The nuclei can be produced by multinucleon transfer (MNT) reactions [15] of a ^{136}Xe beam and ^{198}Pt target system [16]. The electromagnetic moments can be measured by in-gas-cell and gas-jet laser ionization spectroscopy (IGLIS) [17–19].

By employing the MNT reaction combined with KISS, we produced neutron-rich isotopes of refractory elements such as Pt, Ir, Os, Re, W, and Ta and performed nuclear spectroscopy. The search for a laser resonance ionization scheme for refractory elements is currently in progress [20–22]. As a first step, the magnetic dipole moments of ^{199g}Pt ($Z = 78$, $N = 121$, $I^\pi = 5/2^-$, and $t_{1/2} = 30.8(2)$ min) ground state and ^{199m}Pt ($I^\pi = (13/2)^+$, and $t_{1/2} = 13.6(4)$ s) isomeric state [23] were measured by in-gas-cell laser ionization spectroscopy. The nuclear structures of platinum isotopes with $178 \leqslant A \leqslant 198$ have been well studied through measurements of μ, Q, and charge radius by laser spectroscopy [24–28]. In the lighter, neutron-deficient region $178 \leqslant A \leqslant 183$, shape coexistence was found and has been discussed in relation to the charge radii evaluated from the measured isotope shift (IS) [28]. For the heavier region $183 \leqslant A \leqslant 198$, the prolate ($183 \leqslant A \leqslant 188$), triaxial ($190 \leqslant A \leqslant 194$), and oblate ($196 \leqslant A \leqslant 198$) shapes have been discussed and compared with theoretical models [24–27]. In the more neutron-rich region, a spherical shape is dominant toward the shell closure at $N = 126$ in the same way as seen for lead ($Z = 82$) and mercury ($Z = 80$) isotopes [29], predicted by the droplet model [30] with $\beta_2 = 0$. In this paper, we report experimental details and results for in-gas-cell

*yoshikazu.hirayama@kek.jp

laser ionization spectroscopy to determine the magnetic dipole moments of neutron-rich ^{199}Pt.

II. EXPERIMENT

A. Principle of laser spectroscopy for deducing nuclear electromagnetic moments

Laser spectroscopy is a powerful tool for determining nuclear electromagnetic moments through the investigation of hyperfine levels governed by the quantum number F. The possible F values are in the range $|I - J| \leqslant F \leqslant I + J$, where I and J are the nuclear and atomic spins, respectively. According to the F values, if $I > 1/2$, the degenerate atomic energy levels are resolved and shifted by ΔE, which is denoted as follows:

$$\Delta E = \frac{A}{2} \times K + \frac{B}{2} \times \frac{3K(K+1) - 2I(I+1)2J(J+1)}{2I(2I-1)2J(2J-1)},$$
$$K = F(F+1) - I(I+1) - J(J+1). \quad (1)$$

Here, A and B are the magnetic-dipole and electric-quadrupole hyperfine coupling constants, respectively. A and B are related to the nuclear magnetic dipole moment μ and nuclear electric quadrupole moment Q, respectively, and are given by

$$A = \frac{\mu H_{JJ}(0)}{IJ}, \quad (2)$$
$$B = eQ\phi_{JJ}(0) \quad (I, J > 1/2). \quad (3)$$

$H_{JJ}(0)$ and $\phi_{JJ}(0)$ are the magnetic field and the electric field gradient, respectively, induced by the atomic electrons at the position of the nucleus. $H_{JJ}(0)$ and $\phi_{JJ}(0)$ are specific to each atomic state and are common for isotopes. Therefore, the nuclear electromagnetic moments can be evaluated from the measured A and B by using the known A', B', I', μ', and Q' of a specific isotope (generally a stable isotope) as follows:

$$\mu = \frac{I}{I'}\frac{A}{A'}\mu' \quad (4)$$

and

$$Q = \frac{B}{B'}Q' \quad (I, J > 1/2). \quad (5)$$

The atomic energy changes at the ground and excited states, $\Delta E_{\rm gs}$ and $\Delta E_{\rm ex}$, respectively, occur as a result of hyperfine interactions between the nucleus and atomic electrons. The transition frequency between the hyperfine levels of the ground and excited states shifts are

$$\Delta\nu_{\rm i} = \Delta E_{\rm i:ex} - \Delta E_{\rm i:gs} \quad (6)$$

relative to the center of gravity of the fine-structure transition frequency ν_0. From laser spectroscopy measurements of the hyperfine splitting expressed by the $\Delta\nu_{\rm i}$ values, the hyperfine coupling constants A and B, and by extension the electromagnetic moments μ and Q, can be evaluated.

B. Experimental details

1. KISS

The experiment was performed using KISS [13,14], an argon-gas-cell-based laser ion source combined with an online isotope separator, installed in the RIKEN Nishina center. The primary beam ^{136}Xe (10.75 MeV/A, 50 particle-nA), accelerated by the RIKEN Ring Cyclotron, was incident on an enriched ^{198}Pt (purity 91.63%) target with a thickness of 12.5 mg/cm^2. An unstable nucleus ^{199}Pt was produced by a multinucleon transfer reaction [16], and a stable nucleus ^{198}Pt was also emitted from the target by an elastic reaction with ^{136}Xe. In offline tests to study the systematics of the laser ionization for platinum isotopes, stable platinum isotopes ^{192,194,195,196,198}Pt were produced from the resistive heating of a natural platinum filament placed in the gas cell.

The platinum isotopes were accumulated, thermalized, and neutralized in the argon gas cell with a pressure of 88 kPa. The cell was designed to be optimized for efficient gas-flow transportation of neutral isotopes toward the exit [13]. The isotopes were reionized in the gas cell by a two-step resonant laser ionization technique, allowing the atomic number Z to be selected. The laser-produced singly charged ($q = 1$) platinum ions were accelerated with an energy of 20 kV, and their mass-to-charge ratio (A/q) was selected by a dipole magnet. Finally, one kind of isotope was transported to the detector station placed at the neighboring experimental hall.

The detector station includes a tape transport device for avoiding radioactivity in the decay chain of the separated nuclides under pulsed beam operation of the KISS. The radioactive isotope was implanted in an aluminized Mylar tape surrounded by a low-background 32-segmented-proportional gas counter for β-ray detection [31]. This counter works as a β telescope with 16 sets of two layers whose absolute detection efficiency is as high as about 40% for ^{199}Pt β decay due to a lower energy threshold of around 100 keV than typical plastic-scintillator β telescopes. Four super clover Ge detectors, whose absolute detection efficiency for γ rays with an energy of 400 keV is measured to be about 14%, were installed in order to detect β-delayed γ rays and γ rays from the internal transition of isomeric state ^{199m}Pt. The tape was moved at the end of each measurement cycle (every 15 min in the present hyperfine structure [HFS] measurements) to remove unwanted radioactivity from the detection area. The ions of the stable isotopes were counted using a Channeltron detector installed 10 cm upstream from the β-ray telescopes.

2. Laser ionization

Figure 1 shows the ionization scheme and hyperfine structure (HFS) of platinum isotopes. A tunable dye laser (Radiant Dyes Laser; NarrowScan) pumped by a XeCl:excimer laser (λ = 308 nm, Lambda Physik LPX240i) was used for the first-step excitation (λ_1 = 248.792 nm) with a laser power of 70 μJ/pulse. Another XeCl excimer laser of λ_2 = 308 nm with a laser power of 9 mJ/pulse was used for the ionization transition to the continuum above the ionization potential (IP). In the laser ionization spectroscopy, the transition between the ground state $5d\,^9 6s\,^3\mathrm{D}_3$ and the excited state $5d\,^8 6s 6p\,^5\mathrm{F}_4^0$ was studied by scanning the wavelength λ_1. A systematic study of the gas-pressure effects was performed using stable platinum isotopes with mass numbers A = 192, 194, 195, 196, and 198. The pressure broadening and shift in the range 11–88 kPa were measured to be 39(3) MHz/kPa and −22(2) MHz/kPa,

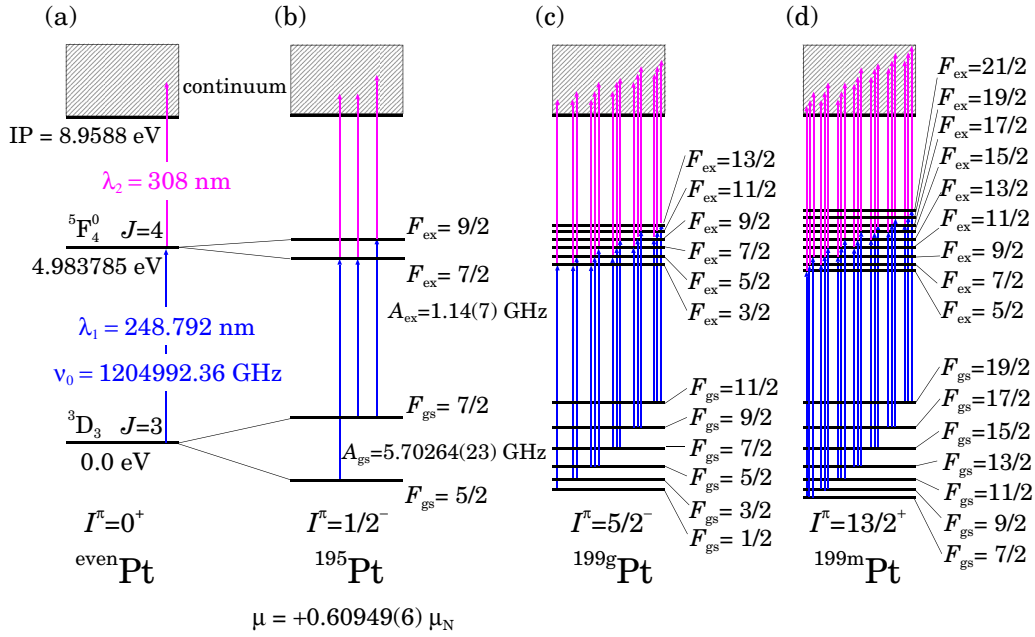

FIG. 1. Ionization scheme and hyperfine structure for platinum isotopes. (a) In the case of ^{even}Pt with $I^\pi = 0^+$, there is no hyperfine splitting. (b) In the case of ^{195}Pt with $I^\pi = 1/2^-$ and $\mu = +0.60949(6)\ \mu_N$, the hyperfine splitting is governed by only A_{gs} and A_{ex}, and there are three transitions. (c) In the case of ^{199g}Pt with $I^\pi = 5/2^-$, the hyperfine splitting of $F_{gs} = 1/2$–$11/2$ and $F_{ex} = 3/2$–$13/2$ is governed by A and B for the ground and excited states, and there are 15 transitions. (d) In the case of ^{199m}Pt with $I^\pi = 13/2^+$ assumed from the systematics of platinum isomeric state, the hyperfine splitting of $F_{gs} = 7/2$–$19/2$ and $F_{ex} = 5/2$–$21/2$ is governed by A and B for the ground and excited states, and there are 21 transitions.

respectively. The isotope shifts for the stable platinum isotopes were also studied.

The excimer lasers were operated at a repetition rate of up to 200 Hz and were synchronized by master trigger signals from a function generator. To produce a UV laser beam as the first-step light, radiation delivered by the NarrowScan was frequency doubled using a barium borate (BBO) crystal placed in a second-harmonic generator. The typical linewidth and pulse width of the dye lasers were 3.4 GHz and 15 ns, respectively. The wavelength was monitored by a wavemeter WS6 (HighFinesse). Ten percent of the UV laser power through a laser beam splitter was monitored during the experiment. The distance between the laser system and the gas cell was about 15 m. Both laser beams, with sizes of about 8–10 mm in diameter, were transported to the gas cell with a small angle and were overlapped in the gas cell for resonance ionization, both spatially and temporally. The spatial overlap was monitored by checking the laser spots in the gas cell using a camera, and it was maintained by adjusting the mirrors with actuators. The temporal overlap was monitored using timing signals from photodetectors measured by an oscilloscope, and it was maintained by adjusting the master trigger signal in 1-ns steps.

III. EXPERIMENTAL RESULTS AND DISCUSSION

A. Identification of ^{199g}Pt and ^{199m}Pt

In the experiment, laser-ionized $^{198}Pt^+$ was first used to adjust the beam-line optics of KISS. Then, the extraction of the laser-ionized radioactive isotope $^{199g}Pt^+$ and $^{199m}Pt^+$ were simultaneously performed by changing the magnetic field of the dipole magnet from $A = 198$ to $A = 199$. The $^{199g}Pt^+$ ($t_{1/2} = 30.8 \pm 0.2$ min [23]) and $^{199m}Pt^+$ ($t_{1/2} = 13.6 \pm 0.4$ s [23]) were identified by measuring the γ rays with the energy of 543 and 392 keV, respectively, as shown in Figs. 2(a) and 2(b).

Half-lives $t_{1/2}$ of the ground and isomeric states were also measured for the firm confirmation of the identifications as shown in Figs. 2(c) and 2(d), respectively. The solid lines in Figs. 2(c) and 2(d) are the best fit result obtained by the fitting routine of the MINUIT code [32] with a fitting function consisting of a single exponential function (with free parameters of amplitude and $t_{1/2}$) and a constant background. After 30 min of irradiation by the $^{199}Pt^+$ beam on the tape, the decay curve was measured over 2.5 h ($\approx 5t_{1/2}$). The measured half-life $t_{1/2} = 31.3 \pm 1.5$ min with the reduced $\chi^2 = 1.19$ is in good agreement with the literature value of $t_{1/2} = 30.8(2)$ min for the ground state, as shown in Fig. 2(c). As a separated measurement, the $t_{1/2}$ of the isomeric state was measured by gating on the 392-keV γ-ray peak as shown in Fig. 2(d). The measured half-life $t_{1/2} = 14.3 \pm 1.4$ s with the reduced $\chi^2 = 0.93$ is also in good agreement with the literature value of $t_{1/2} = 13.6(4)$ s for the isomeric state.

The isomeric ratio $R = Y_{^{199m}Pt}/Y_{^{199g}Pt} = 0.40(5)$ between the extraction yields of the ground state $Y_{^{199g}Pt}$ and isomeric state $Y_{^{199m}Pt}$ was evaluated by analyzing the measured yields of β-delayed γ ray of 543 keV and internal transition γ ray of 392 keV, as shown in Fig. 2(a), during the HFS measurements. $Y_{^{199g}Pt}$ and $Y_{^{199m}Pt}$ were deduced from the integration of the γ-ray yields measured as a function of λ_1. The ratio R was used to analyze the HFS obtained by measuring the β rays.

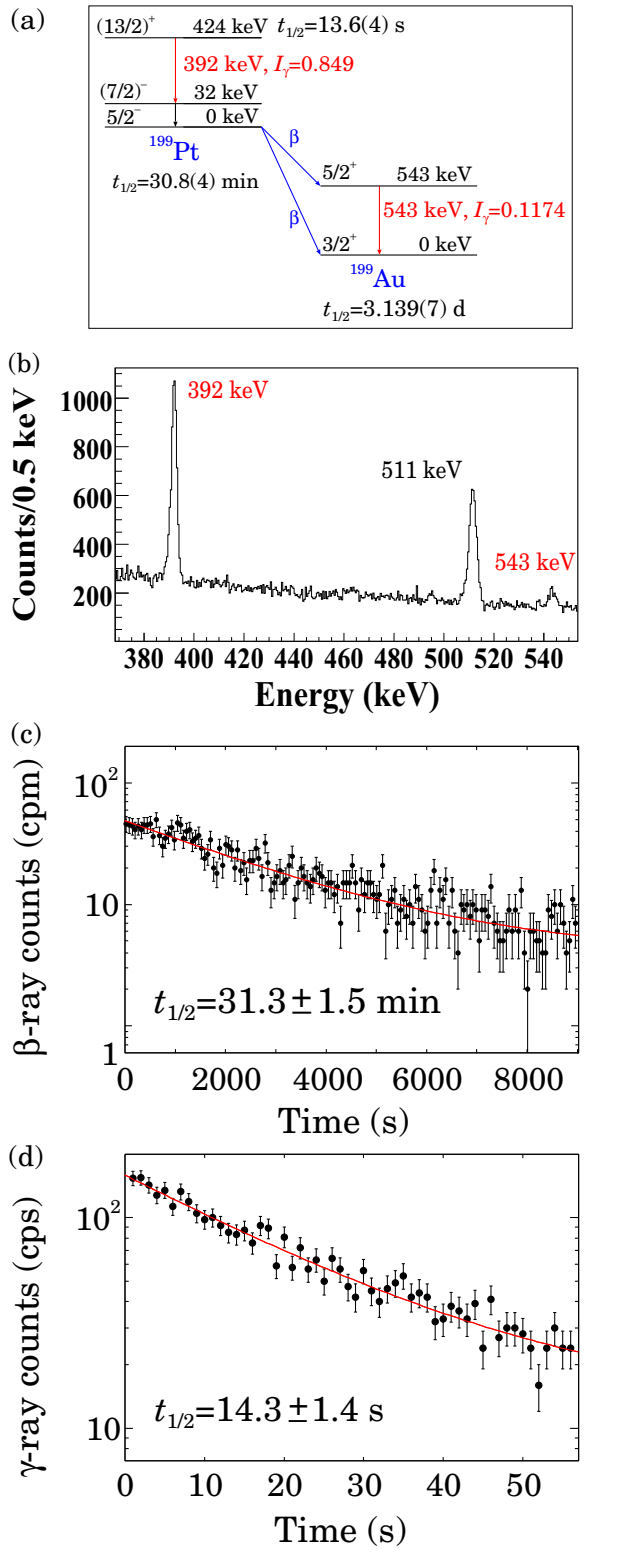

FIG. 2. (a) Schematic decay schemes of ^{199g}Pt and ^{199m}Pt [23]. (b) Energy spectrum of the measured γ rays. Decay γ rays of 392 and 543 keV from the isomeric and ground states were measured, respectively. (c) β decay curve of ^{199g}Pt and (d) internal transition (392-keV γ-ray) decay curve of ^{199m}Pt, which were used for the identifications of ^{199g}Pt and ^{199m}Pt extracted from KISS, respectively.

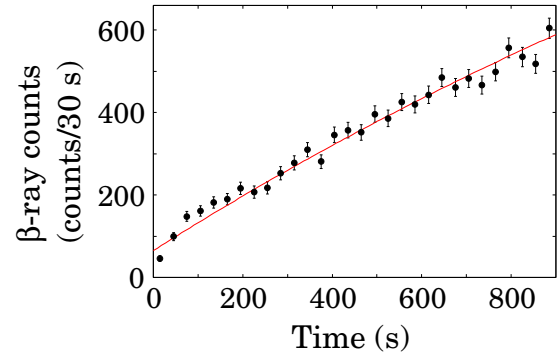

FIG. 3. Typical β-decay growth curve for ^{199}Pt nuclei, which was measured for the evaluation of the extraction yield I_{g+m} of ^{199}Pt nuclei, which consists of the yields of ^{199g}Pt and ^{199m}Pt nuclei.

B. Extraction yields of ^{199g}Pt and ^{199m}Pt

In the present experiment, the extracted yields of ^{199g}Pt and ^{199m}Pt nuclei were measured as functions of the wavelength of λ_1, and the hyperfine splitting was studied to evaluate the magnetic dipole moment.

The extraction yield I_{g+m} was deduced from the growth curve during 15 min of irradiation by measuring β rays, as shown in Fig. 3. The extraction yield I_{g+m} consists of the extraction yields ^{199g}Pt and ^{199m}Pt nuclei from KISS. The solid line in Fig. 3 is the best-fit result with the reduced $\chi^2 = 2.14$, and the fitting function consists of a single exponential function, with the amplitude I_{g+m} as a free parameter, and a constant background under the fixed lifetime of the reported value [23]. Typical reduced χ^2 for each measurement was around 1.5 and in the range of 1–2.5. The fitting error δI_{g+m} was corrected by the square root of the reduced χ^2. The fluctuations of the primary beam intensity within 10%, laser power within 10%, wavelength λ_1 within 0.2 pm, and spatial and temporal overlapping influenced the number of measured β rays emitted from ^{199}Pt nuclei. The growth curve in Fig. 3 reflects the fluctuations, and therefore the evaluated I_{g+m} and its corrected error δI_{g+m} take the fluctuations into account. I_{g+m} and δI_{g+m} were normalized by the measured primary beam dose during each measurement.

The extraction yield I_m of ^{199m}Pt from KISS can be evaluated directly from the measured counts of 392-keV γ ray during 15 min of irradiation. Taking into account the above-mentioned fluctuations, 10% uncertainty of measured I_m was additionally included in δI_m as the systematic error besides the statistical error. I_m and δI_m were also normalized by the measured primary beam dose during each measurement.

Thus, the I_{g+m} and I_m with the related δI_{g+m} and δI_m were independently evaluated from the β-ray and γ-ray measurements, respectively, as a function of the wavelength of λ_1. Finally, the resonance spectra of the HFS for $^{199g+m}$Pt and ^{199m}Pt were obtained as shown in the following section.

C. Data analysis of hyperfine splitting

Figure 4 shows the measured hyperfine splittings of $^{198,195,199m,199g+m}$Pt nuclei extracted from KISS. The line shapes for the resonance peaks were determined from fits of the

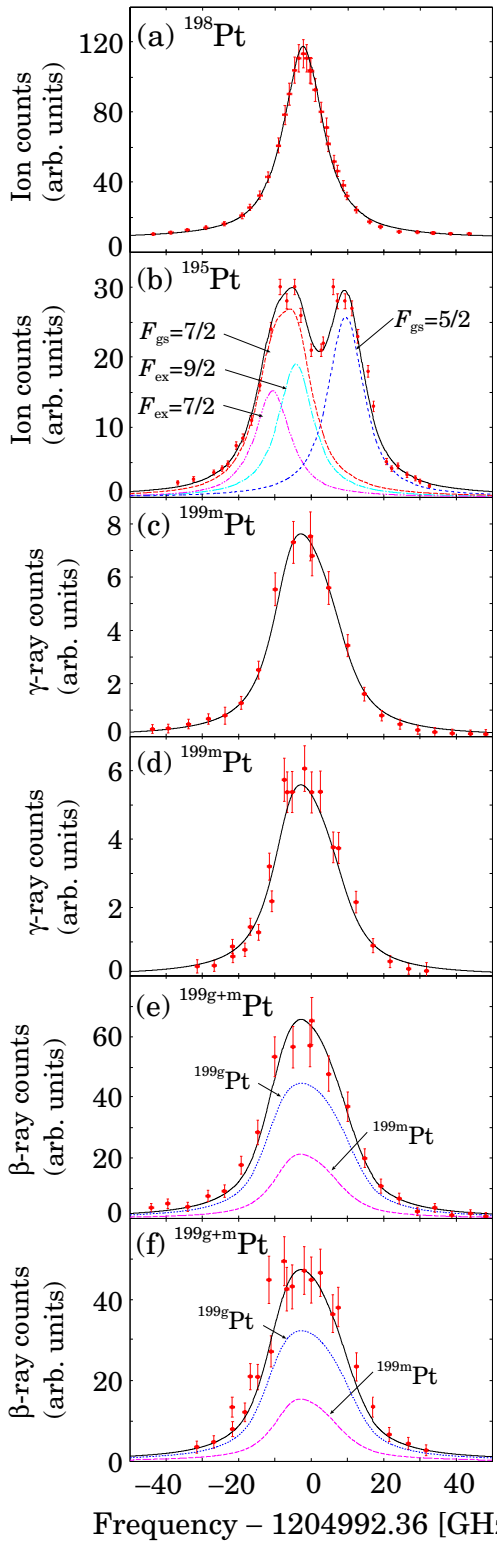

FIG. 4. Measured hyperfine splittings for $^{198,195,199m,199g+m}$Pt nuclei extracted from KISS. Horizontal axis indicates the laser detuning relative to the transition frequency $\nu_0 = 1204992.36$ GHz ($\lambda_1 = 248.792$ nm). The experimental gas pressure and laser power for λ_1 were 88 kPa and 70 μJ/pulse, respectively. (a) The analysis of the single resonance peak of ^{198}Pt nuclei provides the line shape measured under the online experimental conditions. (b) In the HFS spectrum of ^{195}Pt nuclei measured at the offline experiment, the lines labeled by $F_{gs} = 5/2$ and 7/2 indicate transitions from those levels to the excited states. The lines labeled by $F_{ex} = 7/2$ and 9/2 indicate the components of the transitions from $F_{gs} = 7/2$ to those excited hyperfine levels. [(c), (d)] HFS spectra of the ^{199m}Pt nuclei obtained by measuring the yield of 392-keV γ ray. The peaks consist of 21 transitions as shown in Fig. 1(d) from each hyperfine level of $F_{gs} = 7/2, 9/2, 11/2, 13/2, 15/2, 17/2$, and 19/2 in the ground state to the excited states of $F_{ex} = 5/2, 7/2, 9/2, 11/2, 13/2, 15/2, 17/2, 19/2$, and 21/2 in the same manner as the transitions for the ^{195}Pt isotope. [(e), (f)] HFS spectra of the $^{199g+m}$Pt nuclei obtained by evaluating the extraction yield I_{g+m} from the β-decay growth curve as shown in Fig. 3. The peaks consist of 15 transitions as shown in Fig. 1(c) from each hyperfine levels of $F_{gs} = 1/2, 3/2, 5/2, 7/2, 9/2$, and 11/2 in the ground state to the excited states of $F_{ex} = 3/2, 5/2, 7/2, 9/2, 11/2$, and 13/2 in the same manner as the transitions for the ^{195}Pt isotope.

measured single peak of ^{198}Pt ($I^\pi = 0^+$), as shown in Fig. 4(a). The A_{ex} factor for the excited state $5d\,^8 6s6p\,^5F_4^0$ was deduced for the first time from the spectrum analysis of ^{195}Pt ($I^\pi = 1/2^-$ and $\mu = +0.60949(6)\ \mu_N$ [26]) in Fig. 4(b). In order to determine the magnetic dipole moment μ and IS $\delta\nu$, the deduced line shape and A_{ex} were used in the spectrum analysis of ^{199m}Pt and $^{199g+m}$Pt in Figs. 4(c)–4(f). In the analysis, the spectra in Figs. 4(c)–4(f) were simultaneously fitted by using the same functions with the same fitting parameters (Γ_L, μ_i, Q_i, B_{exi}, and $\delta\nu^{198,199i}$) for ^{199i}Pt ($i = g, m$) in order to evaluate the uncertainties of the physics quantities correctly. The details of the analysis are discussed in the following subsections.

1. Line shape

There is no hyperfine splitting for ^{198}Pt with $I^\pi = 0^+$, as shown in Fig. 1(a), and therefore a single resonance peak was observed, as shown in Fig. 4(a). The line shape is a Voigt function, which is a convolution of Gaussian and Lorentzian components. The line shape, as shown in Fig. 4(a), is governed mainly by Lorentzian components in the present experiment. The two Gaussian components are Doppler broadening by an amount governed by the argon gas temperature and laser linewidth, and their full width at half maximum (FWHM) values were evaluated to be 1.0 GHz at 300 K and 3.4 GHz. As a result, a total Gaussian width of 3.5 GHz was obtained and used as a fixed parameter in all the fits. The Lorentzian components consist of gas-pressure broadening, laser-power broadening, and the natural width of 63 MHz of the present transition. The width of the Lorentzian components Γ_L was a free parameter in this analysis, and was deduced to be 12.1(4) GHz. As a result, a total FWHM of 13.1(4) GHz was obtained. The measured line shape for ^{198}Pt in the online experiment was applied to the analyses of other isotopes as a fixed parameter in the fitted functions. The present analysis was performed using the MINUIT code.

2. Hyperfine coupling constant A_{ex}

The hyperfine splitting for ^{195}Pt with $I^\pi = 1/2^-$ and $\mu = +0.60949(6)\ \mu_N$ [23] is governed by A_{gs} and A_{ex}, and there are three transitions, as shown in Fig. 1(b). A_{gs} was precisely measured to be 5.70264(23) GHz [33]. However, A_{ex} for the

excited level was unknown. The fit to the measured spectrum of ^{195}Pt in Fig. 4(b) can provide A_{ex}. The measured line shape for ^{198}Pt was applied to the line shapes for the three transitions, and each resonance peak position as described by Eq. (6) depends only on A_{ex} (here, $B_{gs} = B_{ex} = 0$), which was treated as a free parameter in the analysis.

Another important parameter is the amplitude of each resonance peak. In order to reduce the number of free parameters and constrain the amplitude, the relative intensity [34] for each transition was applied in the present analysis. The relative intensities of the transitions from the $F_{gs} = 5/2$ and 7/2 levels are in proportion to the statistical weights $(2F_{gs}+1)$, and the initial population probabilities in the $F_{gs} = 5/2$ and 7/2 levels are 6/14 $\{= (2\times 5/2+1)/[(2\times 5/2+1)+(2\times 7/2+1)]\}$ and 8/14 $\{= (2\times 7/2+1)/[(2\times 5/2+1)+(2\times 7/2+1)]\}$, respectively. In the present experiment, both the $F_{ex} = 7/2$ and 9/2 levels would be populated by two transitions from $F_{gs} = 7/2$ simultaneously due to the broad line. The relative transition probabilities for the transitions $F_{gs} = 7/2 \rightarrow F_{ex} = 7/2$ and 9/2 are also in proportion to the statistical weights $(2F_{ex}+1)$ of the final states F_{ex}, and are estimated to be 8/18 and 10/18 in the same manner for the initial population probability, respectively. Finally, the relative intensities for the three transitions $F_{gs} = 5/2 \rightarrow F_{ex} = 7/2$, $F_{gs} = 7/2 \rightarrow F_{ex} = 7/2$, and $F_{gs} = 7/2 \rightarrow F_{ex} = 9/2$ are constrained to be $6/14\, f_{amp}$, $8/14\times 8/18\, f_{amp}$, and $8/14\times 10/18\, f_{amp}$, respectively, taking into account the initial population and transition probabilities, and one parameter f_{amp} for the amplitude was used.

The solid black line indicates the best fit to the spectrum in Fig. 4(b), taking into account the isotope shift as a fixed parameter. The IS value was evaluated from the measured values for the ^{192,194,196,198}Pt isotopes, considering the linear relation of the isotope shift [25,26]. The value $A_{ex} = 1.17 \pm 0.10$ GHz for the λ_1 laser power 70 μJ/pulse and 88 kPa gas cell pressure was obtained as a best-fit result. A_{ex} measured for 70 μJ/pulse and 11 kPa, and 240 μJ/pulse and 88 kPa, were 1.05(14) GHz and 1.19(14) GHz, respectively. The deduced A_{ex} values were independent of the experimental conditions, such as the laser power for λ_1 and gas-cell pressure, and were consistent with each other. The weighted averaged $A_{ex} = 1.14 \pm 0.07$ GHz was used for the spectrum analysis of the ^{199}Pt isotope.

3. *Magnetic dipole moments of ^{199g}Pt and ^{199m}Pt*

Figures 4(c) and 4(e) measured during the first frequency scanning and Figs. 4(d) and 4(f) during the second scan show the hyperfine structures for ^{199m}Pt and $^{199g+m}$Pt, respectively.

The hyperfine splittings of the ground and isomeric states are governed by A and B for the ground and excited states, and there are 15 and 21 transitions, respectively, as shown in Fig. 1. Here, we assumed the $I^\pi = 13/2^+$ for ^{199m}Pt from the systematics of platinum isomeric state [23]. Each resonance peak position given by Eq. (6) depends on unknown values of μ_i, Q_i, B_{exi} and IS $\delta\nu^{198,199i}$ between ^{198}Pt and ^{199i}Pt ($i = g,m$) (difference between the shifts from the center of gravity $\nu_0 = 1204992.36$ GHz), which were free parameters in the fitting analysis. Here, B_{gs} of the ground state is related to Q by $B_{gs} = -Q/0.685$ GHz from Ref. [26], and this equation was used in the fitting. The line shape for each transition was fixed to that evaluated in the ^{198}Pt analysis. Taking into account the initial populations in the ground states F_{gs} and the transition probabilities to the excited states F_{gs} evaluated from the statistical weights of $(2F_{gs}+1)$ and $(2F_{ex}+1)$, the relative intensities of the 15 and 21 transitions were constrained in the same manner as the fitting procedure for ^{195}Pt, and one parameter f_{amp} for the amplitude was used. The parameters of the amplitude and background were set free for each spectrum fitting. The isomeric ratio $R = 0.40(5)$ was also taken into account to make constraint on the amplitudes of ^{199g}Pt and ^{199m}Pt in the fitting of spectra [Figs. 4(e) and 4(f)] to fulfill the area ratio between the HFS of ^{199g}Pt and ^{199m}Pt.

The solid black lines in Figs. 4(c)–4(f) indicate the best fit to the spectrum. The measured μ_g, Q_g, and $\delta\nu^{198,199g}$ for the ground state were $+0.75 \pm 0.08$ (stat.) $\pm$ 0.01 (syst.) μ_N, 1.7 $\pm$ 1.7 b, and $+2.13 \pm 0.41$ GHz, respectively. The measured μ_m, Q_m, and $\delta\nu^{198,199m}$ for the isomeric state were -0.57 ± 0.05 (stat.) $\pm$ 0.02 (syst.) μ_N, 3.5 $\pm$ 2.1 b, and $+0.39 \pm 0.39$/GHz, respectively. The B_{ex} was evaluated to be -2.5 ± 5.1/GHz. Here, the fitting errors were corrected by the square root of the reduced χ^2 (=1.03). The systematic error in the magnetic dipole moment stems from the Lorentzian width $\Gamma_L = 12.1(4)$ GHz and hyperfine coupling constant $A_{ex} = 1.14(7)$ GHz deduced from the spectrum analysis of ^{195}Pt in Sec. III C 2. In general, the energy shift induced by B is much smaller than both the energy shift induced by A and the broad resonance width measured by the in-gas-cell laser ionization spectroscopy. This shows that Q and B_{ex} obtained from the present broad spectrum had a minimal influence on the spectrum. The width of the spectrum is mainly governed by the hyperfine splitting induced by the magnetic dipole moments of ^{199g}Pt and ^{199m}Pt. Present spectroscopy therefore enables us to deduce the μ value.

Table I shows the systematics of the magnetic dipole moments of nuclei with $I^\pi = 5/2^-$ and $13/2^+$. The present values of $\mu = +0.75(8)\ \mu_N$ and $\mu = -0.57(5)\ \mu_N$ for ^{199g}Pt and ^{199m}Pt are within the deviation in the measured magnetic dipole moments of nuclei with $I^\pi = 5/2^-$ and $13/2^+$ in this region, respectively, and are consistent with the systematic trend.

4. *Isotope shifts and deformation parameters of ^{199g}Pt and ^{199m}Pt*

The measured IS between ^{198}Pt and ^{199}Pt were $\delta\nu^{198,199g} = +2.13 \pm 0.41$ GHz and $\delta\nu^{198,199m} = +0.39 \pm 0.39$ GHz. Table II shows a summary of the measured IS for the wavelength $\lambda_1 = 248.792$ nm, measured isotopic variation of the mean-square charge radius (these values are referred from Ref. [26]) and quadrupole deformation parameters calculated using the droplet model [30]. The IS between two isotopes with mass number A and A', $\delta\nu^{A,A'} = \nu_0^{A'} - \nu_0^{A}$, is expressed as

$$\delta\nu^{A,A'} = (K_{NMS} + K_{SMS}) \times \frac{m_{A'} - m_A}{m_{A'} m_A} + F_{248} \times \delta\langle r^2\rangle^{A,A'}. \quad (7)$$

Here, K_{NMS} and K_{SMS} are the factors for normal (NMS) and specific (SMS) mass shift components, respectively. The term

TABLE I. Systematics of magnetic dipole moments of nuclei with $I^\pi = 5/2^-$ and $13/2^+$.

Nuclide	I^π	$t_{1/2}$	E_{ex} (keV)	$\mu(\mu_N)$	Q (b)	Method	Ref.
$^{199g}_{78}$Pt	$5/2^-$	30.8(2) min	0	$+0.75 \pm 0.08$[a]	1.7 ± 1.7	IGLIS	Present work
$^{195}_{78}$Pt	$5/2^-$	0.67(3) ns	130	+0.875(100)		Mössbauer	[43]
$^{197}_{78}$Pt	$5/2^-$	16.58(17) ns	53	+0.85(3)		TDPAC	[44]
$^{197}_{80}$Hg	$5/2^-$	8.066(8) ns	134	+0.855(15)	−0.081(6)	TDPAC	[45]
$^{199}_{80}$Hg	$5/2^-$	2.45(5) ns	158	+0.880(33)	+0.95(7)	TDPAC	[45]
$^{199m}_{78}$Pt	$(13/2)^+$	13.6(4) s	424	-0.57 ± 0.05[a]	3.5 ± 2.1	IGLIS	Present work
$^{193}_{78}$Pt	$13/2^+$	4.33(3) d	150	(−)0.753(15)	−0.081(6)	NMR/ON	[40]
$^{195}_{78}$Pt	$13/2^+$	4.02(1) d	259	−0.606(15)	+1.42(60)	NMR/ON[b], NO/CP[c]	[46][b], [41][c]

[a]The errors are summation of the statistic and systematic errors.
[b]For μ measurement.
[c]For sign of μ and Q measurement.

$F_{248} \times \delta\langle r^2\rangle^{A,A'}$ is the field shift (FS) component expressed by the electronic factor F_{248} for the transition $\lambda_1 = 248.792$ nm and the isotopic variation of the mean-square charge radius $\delta\langle r^2\rangle^{A,A'}$.

In order to deduce $\delta\langle r^2\rangle^{A,A'}$ from the measured $\delta\nu^{A,A'}$, Eq. (7) can be practically modified as follows:

$$\delta\langle r^2\rangle^{A,A'}\frac{m_{A'}m_A}{m_{A'}-m_A} = -\frac{K_{MS}}{F_{248}} + \frac{1}{F_{248}}\delta\nu^{A,A'}\frac{m_{A'}m_A}{m_{A'}-m_A}. \quad (8)$$

Here, $K_{MS} = K_{FMS} + K_{SMS}$. If both $\delta\nu^{A,A'}$ and $\delta\langle r^2\rangle^{A,A'}$ for stable isotopes are known, K_{MS} and F_{248} can be evaluated to deduce $\delta\langle r^2\rangle^{A,A'}$ from the measured $\delta\nu^{A,A'}$. Generally, the term of the mass shift (approximately a few 10 MHz) is about two orders of magnitude smaller than the term of the field shift (approximately a few GHz) in the present high $Z = 78$ region [35], and the mass shift term can be neglected in the present case. The factor F_{248} was evaluated to be 17.0 $\pm$ 1.8 GHz/fm^2 from the measured $\delta\nu^{A,A'}$ and $\delta\langle r^2\rangle^{A,A'}$, and the reported $\delta\langle r^2\rangle^{A,A'}$ [26] for ^{even}Pt in Table II by applying Eq. (8). Finally, $\delta\langle r^2\rangle^{194,199g} = 0.268(34)$ and $\delta\langle r^2\rangle^{194,199m} = 0.166(30)$ were obtained from $\delta\nu^{198,199g} = 2.13(41)$ GHz and $\delta\nu^{198,199m} = 0.39(39)$ GHz, respectively. Figure 5 shows the mean square charge radius variation of the platinum isotopes [26,28].

The model-dependent quadrupole deformation parameter $\langle\beta_2^2\rangle$ can be extracted from the measured $\delta\nu^{A,A'}$ and $\delta\langle r^2\rangle^{A,A'}$. The details of the evaluation procedure and its application to platinum isotopes were reported in Refs. [36,26], respectively. The absolute deformation parameters $|\langle\beta_2^2\rangle|^{1/2}$ for

TABLE II. Measured isotope shifts $\delta\nu_{exp}^{194,A}$ and $\delta\nu_{exp}^{198,199}$. Evaluated isotopic variation for the mean-square charge radius $\delta\langle r^2\rangle^{194,199}$ and $\delta\langle r^2\rangle^{194,A}$ from the measured isotope shifts and the reported $\delta\langle r^2\rangle^{194,A}$ in Ref. [26]. Quadrupole deformation parameter $|\langle\beta_2^2\rangle|^{1/2}$ calculated using the droplet model [30].

A	$\delta\nu_{exp}^{194,A}$ [GHz]	$\delta\langle r^2\rangle^{194,A}$ [fm^2]	$\delta\langle r^2\rangle^{194,Ab}$ [fm^2]	$\lvert\langle\beta_2^2\rangle\rvert^{1/2}$
199g	2.13(41)[a]	0.268(34)		0.144(10)
199m	0.39(39)[a]	0.166(30)		0.110(12)
198	2.43(23)	0.143(20)	0.151(6)[b]	0.122(8)
196	1.39(27)	0.082(18)	0.074(4)[b]	0.136(6)
194	0.000	0.000	0.000	0.1434(26)
192	−1.43(27)	−0.084(18)	−0.072(3)[b]	0.150(6)

[a]Measured isotope shift $\delta\nu_{exp}^{198,199}$.
[b]From Ref. [26].

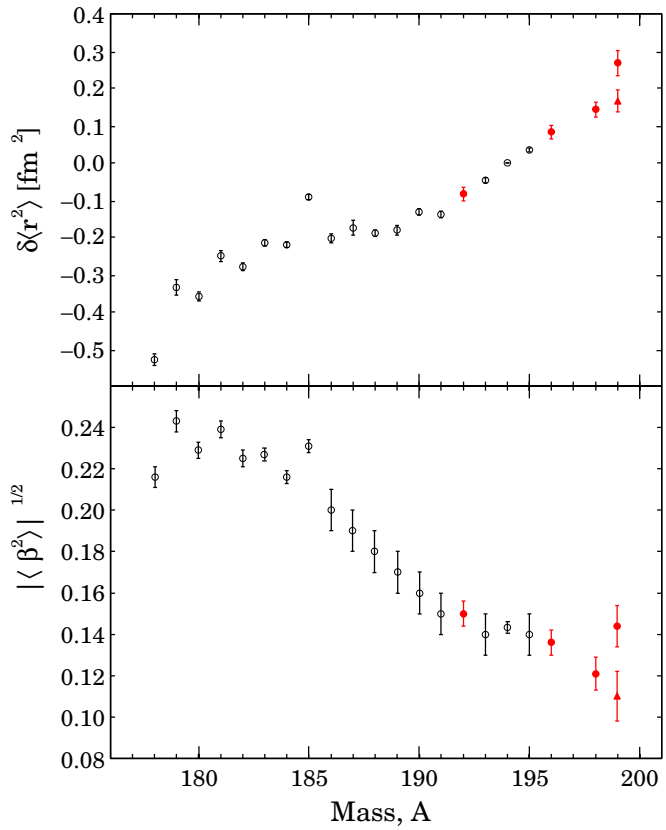

FIG. 5. Systematics of mean square charge radius variation $\delta\langle r^2\rangle^{194,A}$ and quadrupole deformation parameter $|\langle\beta_2^2\rangle|^{1/2}$ as a function of mass number A for platinum isotopes. The open (black) and closed (red) circles represent the values from Ref. [26,28] and the present work, respectively. The closed triangle represents ^{199m}Pt.

^{192,196,198,199g,199m}Pt are listed in Table II. The $\langle\beta_2^2\rangle^A$ was evaluated from Eq. (10), which is derived from Eq. (9) for mass number A and $A = 194$:

$$\langle r^2\rangle^A_{\rm exp} = \langle r^2\rangle^A_{\rm sph} + \frac{5}{4\pi}\langle r^2\rangle^A_{\rm sph}\langle\beta_2^2\rangle^A, \tag{9}$$

$$\langle\beta_2^2\rangle^A = \frac{\delta\langle r^2\rangle^{A,194}_{\rm exp} - \delta\langle r^2\rangle^{A,194}_{\rm sph}}{\frac{5}{4\pi}\langle r^2\rangle^A_{\rm sph}} + \frac{\langle r^2\rangle^{194}_{\rm sph}\langle\beta_2^2\rangle^{194}}{\langle r^2\rangle^A_{\rm sph}}. \tag{10}$$

The $\delta\langle r^2\rangle^{A,194}_{\rm sph}$ and $\langle r^2\rangle^A_{\rm sph}$ for the spherical shape were calculated by using the droplet model [30]. The parameter $\langle\beta_2^2\rangle^{194}$ was deduced from the precisely measured $B(E2,2^+ \to 0^+)$ value of ^{194}Pt [37], and the evaluated parameters $\langle\beta_2^2\rangle$ for $^{\rm even}$Pt were in good agreement with the known $B(E2)$ values [37]. The $|\langle\beta_2^2\rangle|^{1/2}$ for ^{199g}Pt and ^{199m}Pt were evaluated to be 0.144(10) and 0.110(12). The systematic trend of the deformation parameters for $^{193g-199g}$Pt was constant to be around 0.14, and the ground states of the platinum isotopes were oblately deformed. The deformation parameter for ^{199m}Pt was smaller than that for ^{199g}Pt. The deformation for ^{199g}Pt and ^{199m}Pt is discussed in the following section.

D. Discussion

We calculated the low-lying levels of odd platinum isotopes ^{193,195,197,199}Pt by the self-consistent Hartree-Fock-Bogoliubov (HFB) model plus one-quasiparticle excitation built on an even-even HFB vacuum [38]. The SkM* [39] Skyrme energy density functional with time-odd terms and surface-type δ pairing is used. In this way, the effects of core polarization and blocking of a pair of states are self-consistently treated. Then, we calculated the magnetic dipole moments and deformation parameters for the obtained one-quasiparticle states including $I^\pi = 1/2^-, 5/2^-$, and $13/2^+$. The experimental values of $E_{\rm ex}$, μ, and $|\langle\beta_2^2\rangle|^{1/2}$ were compared with the theoretical calculations as shown in Table III.

1. Ground state with $I^\pi = 5/2^-$

The experimental values of $E_{\rm ex}$, μ, and β_2 of ^{193g}Pt$(1/2^-)$, ^{195g}Pt$(1/2^-)$, and ^{197g}Pt$(1/2^-)$ were well reproduced by our systematic HFB + SkM* calculation. The calculation indicates that the ground state with $I^\pi = 1/2^-$ stems from the $[510]1/2^-$ Nilsson orbit. The shapes of ^{193g}Pt$(1/2^-)$, ^{195g}Pt$(1/2^-)$, and ^{197g}Pt$(1/2^-)$ were reported to be oblate [26]. The oblately deformed wave function is essential in order to understand the magnetic dipole moments, taking into account the expectation value of the operator of the magnetic dipole moment. The calculated deformation parameters β_2 were in good agreement with the experimental values and support the interpretation for the magnetic dipole moments.

The μ and β_2 of ^{199g}Pt were calculated using the same framework for the calculations of ^{193g,195g,197g}Pt and were consistent with the experimental values. $I^\pi = 5/2^-$ is naively determined by one valence neutron in a $[503]5/2^-$ orbit, whose Schmidt value is evaluated to be $+1.366\ \mu_{\rm N}$. The present value of $\mu = +0.75(8)\ \mu_{\rm N}$ is about 55% of the Schmidt value. This can be understood from the fact that the magnetic dipole moment of the $[503]5/2^-$ state at oblate deformation gives a smaller value than the Schmidt value of the $2f_{5/2}$ state. The deformation parameter $\beta_2 = -0.095$ obtained from the HFB + SkM* calculation is consistent with the present value of $|\langle\beta_2^2\rangle|^{1/2} = 0.144(10)$. Thus, the oblately deformed shape of ^{199g}Pt explains the present large deviation of the magnetic dipole moment from its Schmidt value. However, the level energy was about 1 MeV above the calculated ground state. In order to check the systematic of μ for the isomeric states of ^{195m1,197m}Pt with $5/2^-$, we calculated the magnetic dipole moments of ^{195m1,197m}Pt$(5/2^-)$ using the same method, but the obtained $\mu = +0.233$ and $+0.354\ \mu_{\rm N}$ values for ^{195m1,197m}Pt$(5/2^-)$ were smaller than the experimental ones, respectively, as shown in Table III.

To reproduce the experimental μ values of ^{195m1,197m}Pt with $5/2^-$, we included the constraint on β_2 value in the above method additionally. By reducing the β_2 values to half, such as $\beta_2 = -0.070$ and -0.055 for ^{195m1,197m}Pt, we obtained $\mu = +0.861$ and $+0.870\ \mu_{\rm N}$, respectively, which are similar to the experimental ones. However, the calculated level energies

TABLE III. Comparison with theoretical calculations. The level with the asymptotic quantum numbers $[Nn_z\Lambda]\Omega^\pi$ corresponds to the blocked level for the one-quasiparticle excitation.

Nuclide	I^π	Exp.			HFB + SkM*			
		$E_{\rm ex}$ [MeV]	μ [μ_N]	$\lvert\langle\beta_2^2\rangle\rvert^{1/2}$	$E_{\rm ex}$ [MeV]	I^π	μ [μ_N]	β_2
^{199g}Pt	$5/2^-$	0	+0.75(8)[a]	0.144(10)[a]	0.981	$[503]5/2^-$	+0.612	−0.095
^{193g}Pt	$1/2^-$	0	+0.603(8)	0.14(1)	0	$[510]1/2^-$	+0.467	−0.157
^{195g}Pt	$1/2^-$	0	+0.60952(6)	0.14(1)	0	$[510]1/2^-$	+0.522	−0.147
^{197g}Pt	$1/2^-$	0	0.51(2)		0	$[510]1/2^-$	+0.673	−0.131
^{195m1}Pt	$5/2^-$	0.130	+0.875(100)		0.412	$[503]5/2^-$	+0.233	−0.140
^{197m}Pt	$5/2^-$	0.053	+0.85(3)		0.477	$[503]5/2^-$	+0.354	−0.124
^{199m}Pt	$(13/2^+)$	0.424	−0.57(5)[a]	0.110(12)[a]	1.55	$[606]13/2^+$	−1.400	+0.088
^{193m}Pt	$13/2^+$	0.150	(−)0.753(15)		1.40	$[606]13/2^+$	−1.299	+0.137
^{195m2}Pt	$13/2^+$	0.259	−0.606(15)		1.53	$[606]13/2^+$	−1.407	+0.126

[a]Present works. The errors are summation of the statistic and systematic errors.

$E_{ex} = 1.954$ and 1.587 MeV for ^{195m1,197m}Pt were deviated about 1.5 MeV from the experimental values. The origin of the energy deviation for the $5/2^-$ state is unclear.

2. Isomeric state with $I^\pi = 13/2^+$

$I^\pi = 13/2^+$ is naively determined by one valence neutron in a $[606]13/2^+$ orbit, whose Schmidt value is evaluated to be $-1.913\ \mu_N$. The present value of $\mu = -0.57(5)\ \mu_N$ is about 30% of the Schmidt value and is much larger than the Schmidt value. The measured μ for Hg, Pb, and Po isotopes with $I^\pi = 13/2^+$ were reported to be approximately $-1.0\mu_N$, which are also about 50% of the Schmidt value. Schütz *et al.* [40] and Scheidemann *et al.* [41] determined the $\mu = (-)0.753(15)\ \mu_N$ of ^{193m}Pt and negative sign of $\mu = -0.606(15)\ \mu_N$ for ^{195m2}Pt, respectively, and suggested that the large deviations originate from a significant difference of static and/or dynamic deformations of Pt isotopes.

The E_{ex}, μ, and β_2 of ^{193m,195m2,199m}Pt$(13/2^+)$ listed in Table III were also calculated by the systematic HFB + SkM* calculation. The calculated E_{ex} was about 1 MeV above the experimental value, and the absolute values of the calculated $|\mu|$ were a factor of about two larger than the measured $|\mu| = 0.57(5)\ \mu_N$. The origin of the energy and μ deviations for the $13/2^+$ state is also unclear. The calculated deformation parameters β_2 are positive, and indicate the prolate deformation for the isomeric states with $I^\pi = 13/2^+$. The Hg and Pb isotopes with $I^\pi = 13/2^+$ were reported to be prolate deformation with $\beta_2 \sim 0.09$ and 0.03 [42], respectively. This systematic was consistent with the present theoretical calculation. The absolute value of the calculated deformation parameter for ^{199m}Pt was smaller than that for ^{199g}Pt, which was also consistent with the present experimental results.

Finally, there are discrepancies between the experimental results such as E_{ex} and μ and theoretical calculations, and this strongly indicates that the experimental values around the $N = 126$ region are required in order to understand the systematic deviation and to improve the effective force.

IV. SUMMARY

Neutron-rich nuclei ^{199g}Pt ($I^\pi = 5/2^-$) and ^{199m}Pt ($I^\pi = 13/2^+$) were produced by a multinucleon transfer reaction at KISS, where nuclear spectroscopy around $N = 126$ is performed for astrophysical and nuclear structure studies. Magnetic dipole moments provide crucial information about the nuclear wave function, which is essential for understanding the competition between allowed Gamow-Teller (GT) and first-forbidden (FF) β-decay transitions in the nuclei around $N = 126$.

By in-gas-cell laser ionization spectroscopy performed at KISS, the magnetic dipole moments μ and mean-square charge radius variations $\delta\langle r^2\rangle^{194,199}$ of ^{199g}Pt and ^{199m}Pt were determined for the first time to be $\mu = +0.75(8)\ \mu_N$ and 0.268(34) fm^2, and $\mu = -0.57(5)\ \mu_N$ and 0.166(30) fm^2, respectively. The measured magnetic dipole moments are consistent with the systematics of those of nuclei with $I^\pi = 5/2^-$ and $13/2^+$ in this region, and the deviations from the Schmidt value due to the oblately deformed wave function for ^{199g}Pt and prolately static or dynamic deformation for ^{199m}Pt, respectively. This interpretation is consistent with the evaluated $|\langle\beta_2^2\rangle|^{1/2} = 0.144(10)$ and 0.110(12) and the reported trend of oblate deformations for $^{193-198}$Pt and prolate deformations for Hg and Pb isotopes, respectively. The evaluated parameters $|\langle\beta_2^2\rangle|^{1/2}$ for platinum isotopes are consistent with the linear relation for platinum isotopes with $193 \leqslant A \leqslant 198$. The behavior with increasing neutron number toward $N = 126$ indicates a change to a spherical shape for the platinum isotopes.

A systematic nuclear spectroscopy study is planned for neutron-rich isotopes of refractory elements such as Pt, Ir, Os, Re, W, and Ta by employing the MNT reaction combined with KISS. Once reaction products are neutralized in the gas cell, the in-gas-cell laser ionization technique can easily be applied to about 80% of elements to study electromagnetic moments and charge radii. Moreover, state-of-the-art laser systems combined with a narrow-band technique enables in-gas-jet laser ionization spectroscopy for precise measurements of these values.

ACKNOWLEDGMENTS

This experiment was performed at the RI Beam Factory operated by RIKEN Nishina Center and CNS, University of Tokyo. The authors wish to acknowledge the staff of the accelerator for their support. This work was supported by JSPS KAKENHI Grants No. JP23244060, No. JP24740180, No. JP26247044, and No. JP15H02096.

[1] I. N. Borzov, Phys. Rev. C **67**, 025802 (2003).
[2] P. Möller, B. Pfeiffer, and K.-L. Kratz, Phys. Rev. C **67**, 055802 (2003).
[3] H. Koura, T. Tachibana, M. Uno, and M. Yamada, Prog. Theor. Phys. **113**, 305 (2005).
[4] P. Möller, J. R. Nix, and K.-L. Kratz, At. Data Nucl. Data Tables **66**, 131 (1997).
[5] J. Engel, M. Bender, J. Dobaczewski, W. Nazarewicz, and R. Surman, Phys. Rev. C **60**, 014302 (1999).
[6] G. Martinez-Pinedo, Nucl. Phys. A **688**, 357 (2001).
[7] K. Langanke and G. Martinez-Pinedo, Rev. Mod. Phys. **75**, 819 (2003).
[8] KUTY, http://wwwndc.jaea.go.jp/nucldata/beta-decay-properties.pdf.
[9] E. M. Burbidge, G. R. Burbidge, W. A. Fowler, and F. Hoyle, Rev. Mod. Phys. **29**, 547 (1957).
[10] M. R. Mumpower, R. Surman, G. C. McLaughlin, and A. Aprahamian, Prog. Part. Nucl. Phys. **86**, 86 (2016).
[11] N. J. Stone, At. Data Nucl. Data Tables **90**, 75 (2005).

[12] S. C. Jeong, N. Imai, H. Ishiyama, Y. Hirayama, H. Miyatake, and Y. X. Watanabe, KEK Rep. 2010-2, 2010, https://lib-extopc.kek.jp/preprints/PDF/2010/1024/1024002.pdf.
[13] Y. Hirayama, Y. X. Watanabe, N. Imai, H. Ishiyama, S. C. Jeong, H. Miyatake, M. Oyaizu, S. Kimura, M. Mukai, Y. H. Kim *et al.*, Nucl. Instrum. Methods Phys. Res., Sect. B **353**, 4 (2015).
[14] Y. Hirayama, Y. X. Watanabe, N. Imai, H. Ishiyama, S. C. Jeong, H. S. Jung, H. Miyatake, M. Oyaizu, S. Kimura, M. Mukai *et al.*, Nucl. Instrum. Methods Phys. Res., Sect. B **376**, 52 (2016).
[15] C. H. Dasso, G. Pollarolo, and A. Winther, Phys. Rev. Lett. **73**, 1907 (1994).
[16] Y. X. Watanabe, Y. H. Kim, S. C. Jeong, Y. Hirayama, N. Imai, H. Ishiyama, H. S. Jung, H. Miyatake, S. Choi, J. S. Song *et al.*, Phys. Rev. Lett. **115**, 172503 (2015).
[17] T. E. Cocolios, A. N. Andreyev, B. Bastin, N. Bree, J. Büscher, J. Elseviers, J. Gentens, M. Huyse, Y. Kudryavtsev, D. Pauwels *et al.*, Phys. Rev. C **81**, 014314 (2010).
[18] R. Ferrer, N. Bree, T. E. Cocolios, I. G. Darby, H. De Witte, W. Dexters, J. Diriken, J. Elseviers, S. Franchoo, M. Huyse *et al.*, Phys. Lett. B **728**, 191 (2014).
[19] Y. Kudryavtsev, R. Ferrer, M. Huyse, P. V. den Bergh, and P. V. Duppen, Nucl. Instrum. Methods Phys. Res., Sect. B **297**, 7 (2013).
[20] Y. Hirayama, M. Mukai, Y. X. Watanabe, N. Imai, H. Ishiyama, S. C. Jeong, H. Miyatake, M. Oyaizu, Y. Matsuo, T. Sonoda, and M. Wada, J. Phys. B **47**, 075201 (2014).
[21] M. Mukai, Y. Hirayama, N. Imai, H. Ishiyama, S. C. Jeong, H. Miyatake, M. Oyaizu, Y. X. Watanabe, Y. H. Kim, and S. Kimura, JPS Conf. Proc. **6**, 030127 (2015).
[22] M. Mukai, Y. Hirayama, H. Ishiyama, H. S. Jung, H. Miyatake, M. Oyaizu, Y. X. Watanabe, S. Kimura, A. Ozawa, S. C. Jeong, and T. Sonoda, Nucl. Instrum. Methods Phys. Res., Sect. B **376**, 73 (2016).
[23] R. B. Firestone, *Table of Isotopes* (John Wiley & Sons, New York, 1996).
[24] J. K. P. Lee, G. Savard, J. E. Crawford, G. Thekkadath, H. T. Duong, J. Pinard, S. Liberman, F. Le Blanc, P. Kilcher, J. Obert *et al.*, Phys. Rev. C **38**, 2985 (1988).
[25] H. T. Duong, J. Pinard, S. Liberman, G. Savard, J. K. P. Lee, J. E. Crawford, G. Thekkadath, F. L. Blanc, P. Kilcher, J. Obert *et al.* (ISOLDE Collaboration), Phys. Lett. B **217**, 401 (1989).
[26] T. Hilberath, S. Becker, G. Bollen, H.-J. Kluge, U. Krönert, G. Passler, J. Rikovska, R. Wyss *et al.* (ISOLDE Collaboration), Z. Phys. A: Hadrons Nucl. **342**, 1 (1992).
[27] P. Kilcher, J. C. Putaux, J. E. Crawford, H. Dautet, H. T. Duong, F. L. Blanc, J. K. P. Lee, J. Obert, J. Oms, J. Pinard *et al.*, Nucl. Instrum. Methods Phys. Res., Sect. B **70**, 537 (1992).
[28] F. Le Blanc, D. Lunney, J. Obert, J. Oms, J. C. Putaux, B. Roussière, J. Sauvage, S. Zemlyanoi, J. Pinard, L. Cabaret *et al.*, Phys. Rev. C **60**, 054310 (1999).
[29] H. De Witte, A. N. Andreyev, N. Barrè, M. Bender, T. E. Cocolios, S. Dean, D. Fedorov, V. N. Fedoseyev, L. M. Fraile, S. Franchoo *et al.*, Phys. Rev. Lett. **98**, 112502 (2007).
[30] W. D. Myers and K.-H. Schmidt, Nucl. Phys. A **410**, 61 (1983).
[31] M. Mukai, Y. Hirayama, Y. X. Watanabe *et al.* (unpublished).
[32] CERN Program Library entry D506.
[33] S. Büttgenbach, N. Glaeser, B. Roski, and R. Träber, Z. Phys. A: At. Nucl. **317**, 237 (1984).
[34] U. Köster, N. J. Stone, K. T. Flanagan, J. R. Stone, V. N. Fedosseev, K. L. Kratz, B. A. Marsh, T. Materna, L. Mathieu, P. L. Mokkanov *et al.*, Phys. Rev. C **84**, 034320 (2011).
[35] K. Blaum, J. Dilling, and W. Nörtershäuser, Phys. Scr., **T152**, 014017 (2013).
[36] S. Ahmad, W. Klempt, C. Ekström, R. Neugart, K. Wendt *et al.* (ISOLDE Collaboration), Z. Phys. A: At. Nucl. **321**, 35 (1985).
[37] S. Raman, J. Nestor, S. Kahane, and K. Bhatt, At. Data Nucl. Data Tables **42**, 1 (1989).
[38] M. Bender, P. Bonche, T. Duguet, and P.-H. Heenen, Nucl. Phys. A **723**, 354 (2003).
[39] J. Bartel and P. Quentin, Nucl. Phys. A **386**, 79 (1982).
[40] G. Schütz, E. Hagn, P. Kienle, and E. Zech, Phys. Rev. Lett. **56**, 1051 (1986).
[41] E. Scheidemann, R. Eder, E. Hagn, and E. Zech, Z. Phys. A **340**, 235 (1991).
[42] G. Neyens, Rep. Prog. Phys. **66**, 633 (2003).
[43] B. Wolbeck and K. Zioutas, Nucl. Phys. A **181**, 289 (1972).
[44] R. N. Saxena and J. C. Soares, Hyperfine Interact. **9**, 93 (1981).
[45] K. Krien, K. Kroth, H. Saitovitch, and W. Thomas, Z. Phys. A **283**, 337 (1977).
[46] F. Bacon, G. Kaindl, H.-E. Mahnke, and D. Shirley, Phys. Rev. Lett. **28**, 720 (1972).